Flux Leakage Analytical Calculation in the E-shape Stator of Linear Rotary Motor with Interlaced Permanent Magnet Poles

Kaikai Guo[1], Youguang Guo[2] and Shuhua Fang[3]

[1]School of Electrical and Information Engineering, Anhui University of Science and Technology, Huainan, 232001, China
[2]School of Electrical and Data Engineering, University of Technology Sydney, Sydney, NSW, 2007, Australia
[3]School of Electrical Engineering, Southeast University, Nanjing 210096, China

The circumferential and axial widths of permanent magnet (PM) pole and E-shape stator pole of linear rotary motor with interlaced PM poles are very influential to the back electromotive force (EMF) and the flux leakage analysis is complex, which causes difficulty in optimization of the motor structure. One of the key issues in optimization design is to calculate the flux leakage accurately. In this paper, the main flux and side flux variation laws of stator pole are derived by analytical method. The flux leakage can be divided into the flux leakage between the PM and the mover, flux leakage on the stator tooth tip and the flux leakage between the adjacent PM poles and stator pole. The 3D flux leakage calculation model is built, which is suitable for the calculation of magnetic flux based on different motor operating principles. Then the rotational and rectilinear back EMFs are calculated by analytical method, which are consistent with the results analyzed by 3-D finite element method.

***Index Terms*—Analytical method, Finite element method, Flux leakage, Linear rotary machine**

I. Introduction

LINEAR rotary motor (LRM) can be used in many fields, such as machine numerical control and electric drill. There are still many problems to be solved in the process of optimization design, which has been studied by many scholars. The calculation of the magnetic field distribution is very important in the motor design. Many methods are presented, such as subdomain method [1], analytical method [2-4], finite element method (FEM) [5] and the combined method [6][7]. The subdomain method can accurately predict the magnetic flux density, and it was used in the analysis of the electromagnetic characteristics of a slotless segmented-Halbach permanent magnet (PM) synchronous machine (SM) in [1]. The magnetic flux distributions of single-cage induction machines were calculated by analytical method in [2]. The optimizations of cogging torque and detent force of a linear rotary PM motor were analyzed based on the study of air gap flux density calculated by 3-D analytical method [3][4] and FEM [5], respectively. In [6], the air-gap flux densities of surface-mounted PM machines and transverse flux motor were analyzed based on the method by combining the magnetic circuit method (MCM) and subdomain method. An analytical approach to determine the phase inductance of a switched reluctance machine with any common topologies, dimensions and phase currents at any rotor position was proposed in [7] by combining the Maxwell's equations and magnetic network methods, which can consider the impact of the saturation effects of steel on the phase inductance profile.

The back electromotive force (EMF) is an important characteristic index in the optimal design of the motor. However, it is difficult to calculate the back EMF because of the flux leakages. The flux linkage characteristics of the switched reluctance linear generator was analyzed based on the neural networks with the relationship between the mover position and the phase current [8]. A multiloop method was presented to calculate the current distribution and the inductances of a salient pole SM with internal faults based on the voltage equation of a single coil in the stator winding in [9]. The air-gap and zigzag flux leakages in a surface-mounted PM machine were analyzed to predict the flux distribution in [10]. In order to analyze the tooth-tip flux leakage, the magnetic equivalent network of a PM linear vernier machine was analyzed, which can consider the air-gap fringing effect [11]. The no-load flux leakage coefficient of an interior PMSM was calculated by establishing the analytical model in [12].

The circumferential and axial back EMFs of LRM with interlaced PM (IPM) poles are important characteristic indexes, which must be considered in the optimal design. Since the circumferential and axial widths of PM pole and stator pole are very influential to the back EMF and the flux leakages in the circumferential and axial directions are complex, the main flux and the total side flux of E-shape stator are calculated based on the calculated results of air gap flux density by analytical method. The 3-D flux leakage calculation model is built, which can calculate the flux leakage between the PM pole and the mover, the flux leakage between the adjacent PM poles, and the flux leakage between the PM poles and stator pole. Then the flux leakage of each stator pole can be derived and the back EMF can be taken as the optimization objective. According to the analytical results of air gap flux density in [3] and relative magnetic permeance in [4], the minimum values of the amplitudes of cogging torque and detent force are also taken as the optimization objectives.

II. Flux Characteristics Analysis of IPM-LRM

A. Topology of IPM-LRM

Fig. 1 shows the topology of IPM-LRM. The six axial E-type stator sections are arrayed in the circumferential direction, and the interlaced PM poles are mounted on the surface of the mover. Rotational and linear movements are implemented by only one magnetic circuit based on the transverse flux principle and electromagnetic induction

Manuscript

principle, respectively.

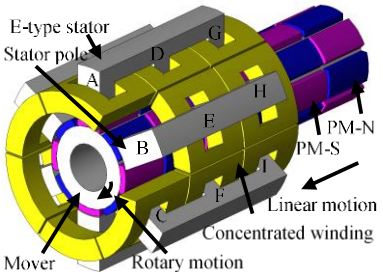

Fig. 1. Topology of IPM-LRM.

B. Flux Characteristics Analysis

Fig. 2 shows the flux leakage analysis model of the IPM-LRM. The flux leakage contains the PM-PM leakage (*a*, *e*), PM-mover leakage (*b*, *f*) and PM-stator pole-PM (*c*, *d*). S_{A1}, S_{A2}, S_{A3}, S_{A4}, S_{D1}, S_{D2}, S_{D3}, S_{D4}, S_{E1}, S_{E2}, S_{E3} and S_{E4} are the side faces of stator poles *A*, *D* and *E*, respectively. When the motor works in rotary motion, the side fluxes of S_{A2}, S_{A4}, S_{D2}, S_{D4}, S_{E2} and S_{E4} are decided by the axial position of the mover, and the side fluxes of S_{A1}, S_{A3}, S_{D1}, S_{D3}, S_{E1} and S_{E3} are decided by the circumferential position of the mover. The main flux and tooth top flux leakage are emitted by PM poles, and enter the stator core through the air gap, and then return to the PM through the air gap. Due to the influence of the stator slots, the air gap flux density distribution is not uniform and the value is unknown, there are large flux leakage in regions (*a*, *b*, *c*, *d*, *e*, *f*), so it is difficult to calculate the flux accurately.

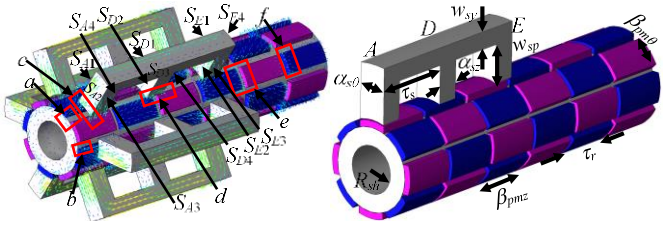

Fig. 2. Flux leakage analysis model of the IPM-LRM, (a) magnetic vector plot, and (b) single stator diagram.

III. Magnetic Field Calculation

A. Calculation of Flux Linkage at Side Face

Fig. 3 shows the model of IPM-LRM without stator slots. Air_I and PM_{II} are the air gap region and PM region, respectively. R_s, R_m and R_r are the inner radius of the stator, the outer radii of PM and mover, respectively.

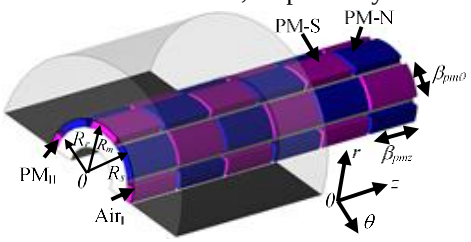

Fig. 3. Model of IPM-LRM without stator slots.

The stator tooth flux can contain the main flux, side flux and part flux leakage, and the main flux expression of the stator tooth of phase *A* is

$$\phi_{Am}=\int_{-\alpha_{sz}/2}^{\alpha_{sz}/2}\int_{-\pi\alpha_{sp}/2p}^{\pi\alpha_{sp}/2p} B_{Ir}(r,\theta,z)\cdot\pi\alpha_{sp}\alpha_{sz}\,/\,pd\theta dz \tag{1}$$

where $\alpha_{s\theta}$ and α_{sz} are the widths of stator pole in the circumferential and axial directions, respectively. α_{sp} is the pole arc coefficient of stator pole in the circumferential direction. $\alpha_{s\theta}=2(R_m+g)\sin(\alpha_{sp}/2)$. Ignoring the effects of magnetic field frequency and eddy currents, the air gap flux density of IPM-LRM without stator slots as shown in Fig. 3 is solved by the separation of variables method in [3]. The expression of air gap flux density in Air_I region in radial direction is

$$\begin{aligned}B_{Ir}(r,\theta,z)&=-\mu_0\frac{\partial\phi_I(r,\theta,z)}{\partial r}\\&=-\sum_{i=1,3,5\cdots}^{\infty}\sum_{j=1,3,5\cdots}^{\infty}[A_I I_v'(\upsilon r)+K_v'(\upsilon r)]\cos(ip\theta)\cos(j\pi z/\tau_r)\\&=-\sum_{i=1,3,5\cdots}^{\infty}\sum_{j=1,3,5\cdots}^{\infty}\frac{A_I}{K_v(\upsilon R_s)}[I_v'(\upsilon r)K_v(\upsilon R_s)-I_v(\upsilon R_s)K_v'(\upsilon r)]\\&\quad\cos(ip\theta)\cos(j\pi z/\tau_r)\end{aligned} \tag{2}$$

where

$$\begin{aligned}A_I=\frac{\begin{aligned}&\{-[\phi_{ij}^*K_v'(\upsilon R_m)-\frac{M_{i,j}}{\mu_r}K_v(\upsilon R_m)]I_v(\upsilon R_r)K_v(\upsilon R_s)\\&-\phi_{ij}^*K_v(\upsilon R_s)[K_v(\upsilon R_m)I_v'(\upsilon R_m)-K_v'(\upsilon R_m)I_v(\upsilon R_m)]\\&+[\phi_{ij}^*I_v'(\upsilon R_m)-\frac{M_{i,j}}{\mu_r}I_v(\upsilon R_m)]K_v(\upsilon R_s)K_v(\upsilon R_r)\}\end{aligned}}{\begin{aligned}&[I_v(\upsilon R_s)K_v(\upsilon R_r)-I_v(\upsilon R_r)K_v(\upsilon R_s)]\\&[K_v'(\upsilon R_m)I_v(\upsilon R_m)-K_v(\upsilon R_m)I_v'(\upsilon R_m)]\end{aligned}}\end{aligned}$$

The side flux of stator pole contains the effective flux and part flux leakage, which is difficult to calculate. Taking the E-shape stator as a whole analysis objective, Fig. 4 shows the magnetic vector diagram of IPM-LRM when the side flux reaches the minimum value. Figs. 4 (a), (b) and (c) are the positions when the third, the second and the first stator poles of E-shape stator are align with the centerline of the adjacent PM poles in axial directions, respectively. z_{00}, z_{01} and z_{02} are the distances between the E-type stator edge and the rotor edge when the stator flux reaches the minimum values in linear motion.

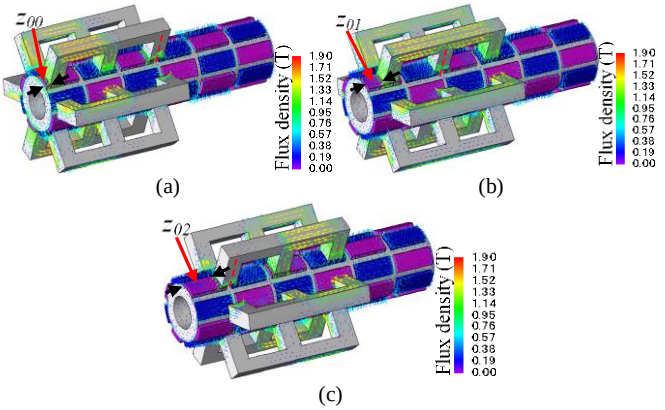

Fig. 4. Magnetic vector diagram when the side flux reaches the minimum value, (a) centerline of phase *G*, (b) centerline of phase *D*, and (c) centerline of phase *A* consistent with the centerline of the air gap between the PM poles in axial direction.

Fig. 2 (b) shows the main structure diagram of IPM-LRM with single stator section. τ_s and τ_r are the pole pitch of stator pole and PM pole in the axial directions, respectively. Since the 3/4 pole-slot combination form is adopted in the linear

motion, the expression $3\tau_s=4\tau_r$ can be derived. According to the positions in Figs. 4 (a) and (c), the following expressions can be obtained

$$\begin{cases} 3\cdot\tau_r = 2\cdot\tau_s + z_{00} + \alpha_{sz}/2 \\ \tau_r = z_{02} + \alpha_{sz}/2 \end{cases} \tag{3}$$

Then

$$k_z = 2\cdot\tau_r/(z_{02}-z_{00}) = 3 \tag{4}$$

The expression of the total side flux of phases *A*, *D* and *G* is

$$\begin{aligned} \phi_S &= \phi_{S_{A1}} + \phi_{S_{A2}} + \phi_{S_{A3}} + \phi_{S_{A4}} + \phi_{S_{D1}} + \phi_{S_{D2}} \\ &\quad + \phi_{S_{D3}} + \phi_{S_{D4}} + \phi_{S_{G1}} + \phi_{S_{G2}} + \phi_{S_{G3}} + \phi_{S_{G4}} \\ &= \phi_{S\max}(\theta,z)\sin(w_\theta\theta+\theta_{0s})\sin(k_z w_z z + z_{0s}) \end{aligned} \tag{5}$$

where ϕ_{Smax} is the maximum value of the total side flux of E-shape stator, ω_θ and ω_z are the angular velocities in the circumferential and axial directions, respectively. θ_{0s} and z_{0s} are the initial phases of the side flux in circumferential and axial directions, respectively.

B. Calculation of Flux Leakage

Fig. 5 shows the flux leakage calculation model of single stator pole. The calculations of PM-PM leakage, PM-mover leakage and PM-stator pole-PM leakage are complex, which need to consider the widths of stator pole and PM pole in circumferential and axial directions. R_{m0} is the internal reluctance of a PM pole, $R_{pM\theta}$ and R_{pMz} are the leakage reluctance between a pole PM and the mover in circumferential and axial directions, respectively. $R_{pp\theta}$ and R_{ppz} are the leakage reluctance between adjacent PM poles in circumferential and axial directions, respectively. $R_{psp\theta}$ and R_{pspz} are the leakage reluctance between adjacent PM poles and the stator pole in circumferential and axial directions, respectively.

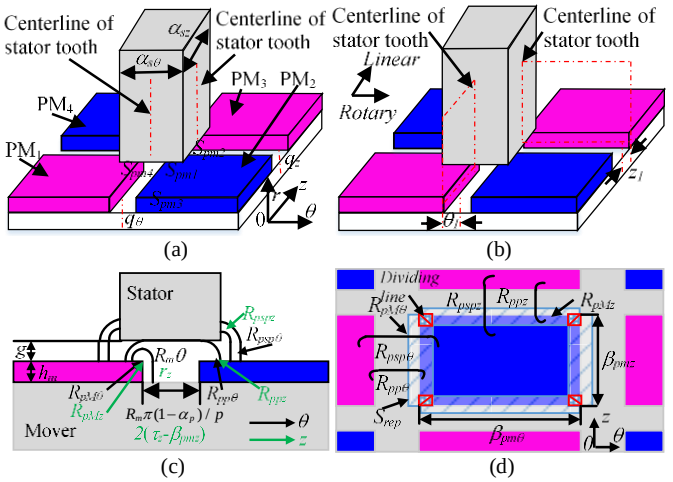

Fig. 5. Flux leakage calculation model of single stator pole, (a) the initial position, (b) calculation model, (c) cross section diagram, and (d) top view of single tooth calculation model.

The flux leakage decreases by half along the dividing line in circumferential and axial directions in the overlapping region, which is shown in Fig. 5 (d). In order to avoid the overlap of the calculation area of circular leakage and axial leakage of PM, the upper limit of the integration in the circumferential and axial directions are separately reduced by one δ. The expressions of the flux leakage magnetic permeance between the PM pole and the mover ($P_{pM\theta}$, P_{pMz}) of single PM pole along the circumferential and axial directions are

$$P_{pM\theta} = \int_0^{\beta_{pmz}-\delta}\int_0^{\frac{\delta}{R_m}} \frac{\mu_0 R_m d\theta dz}{\pi R_m\theta + h_m} = \frac{\mu_0(\beta_{pmz}-\delta)}{\pi}\ln\frac{\pi\delta+h_m}{h_m} \tag{6}$$

$$P_{pMz} = \int_0^{\frac{\pi}{p}\alpha_p-\frac{\delta}{R_m}}\int_0^{\delta} \frac{\mu_0 dr_z d\theta}{\pi r_z + h_m} = (\frac{\mu_0\alpha_p}{p} - \frac{\mu_0\delta}{\pi R_m})\ln\frac{\pi\delta+h_m}{h_m} \tag{7}$$

The expressions of the flux leakage magnetic permeance of between the adjacent PM poles ($P_{pp\theta}$, P_{ppz}) of single PM pole in the circumferential and axial directions are

$$\begin{aligned} P_{pp\theta} &= \int_0^{\beta_{pmz}-\delta}\int_0^{\frac{\delta}{R_m}} \frac{\mu_0 R_m d\theta dz}{\pi R_m\theta + \pi R_m(1-\alpha_p)/p} \\ &= \frac{\mu_0(\beta_{pmz}-\delta)}{\pi}\ln\frac{\pi p\delta + R_m\pi(1-\alpha_p)}{R_m\pi(1-\alpha_p)} \end{aligned} \tag{8}$$

$$\begin{aligned} P_{ppz} &= \int_0^{\frac{\pi}{p}\alpha_p-\frac{\delta}{R_m}}\int_0^{\delta} \frac{\mu_0 dr_z d\theta}{\pi r_z + 2(\tau_z-\beta_{pmz})} \\ &= (\frac{\mu_0\alpha_p}{p} - \frac{\mu_0\delta}{\pi R_m})\ln\frac{\pi\delta+2(\tau_z-\beta_{pmz})}{2(\tau_z-\beta_{pmz})} \end{aligned} \tag{9}$$

When the *q*-axis aligns with the centerline of the stator tooth in the circumferential and axial directions, the flux leakage can reach the maximum value as shown in Fig. 5(a), which can be taken as the initial position. Since the flux leakage of PM-stator pole-PM is related with the relative position of the stator and the mover, pole pitches in circumferential and axial directions, and the corresponding relationship values of z_1 and z_z are shown in Table I. The corresponding relationship values of θ_1 and θ_z are shown in Table II. g is the air gap width. The expressions of the flux leakage magnetic permeance of PM-stator pole-PM in the circumferential and axial directions are

$$P_{psp\theta}(\theta_1,z_1) = \begin{cases} \displaystyle\int_0^{z_z}\int_0^{\frac{\delta}{R_m}} \frac{\mu_0 R_m d\theta dz}{\pi R_m\theta+g} \\ 0<\theta_1<\pi(\alpha_{sp}-1+\alpha_p)/2p \ \ or \ \ \pi(2-\alpha_p-\alpha_{sp})/2p<\theta_1<\pi/p \\ \displaystyle\int_0^{z_z}\int_{\theta_1-\frac{\pi}{2p}(\alpha_{sp}-1+\alpha_p)}^{\frac{\delta}{R_m}} \frac{\mu_0 R_m d\theta dz}{\pi R_m\theta+g} \quad \frac{\pi(\alpha_{sp}-1+\alpha_p)}{2p}<\theta_1<\frac{\pi\alpha_{sp}}{2p} \\ \displaystyle\int_0^{z_z}\int_{\frac{\pi(3-\alpha_p-\alpha_{sp})}{2p}-\theta_1}^{\frac{\delta}{R_m}} \frac{\mu_0 R_m d\theta dz}{\pi R_m\theta+g} \quad \frac{\pi(2-\alpha_{sp})}{2p}<\theta_1<\frac{\pi(3-\alpha_p-\alpha_{sp})}{2p} \end{cases} \tag{10}$$

$$P_{pspz}(\theta_1, z_1) = \begin{cases} \int_0^{\theta_\theta}\int_0^{\delta} \dfrac{\mu_0 dr_z d\theta}{\pi r_z + g} \\ 0 < z_1 < (\alpha_{sz} - \tau_r + \beta_{pmz})/2 \; or \; (3\tau_r - \beta_{pmz} - \alpha_{sz})/2 < z_1 < \tau_r \\ \int_0^{\theta_\theta}\int_{z_1 - \frac{\alpha_{sz}-\tau_r+\beta_{pmz}}{2}}^{\delta} \dfrac{\mu_0 dr_z d\theta}{\pi r_z + g} \quad \dfrac{\alpha_{sz} - \tau_r + \beta_{pmz}}{2} < z_1 < \dfrac{\alpha_{sz}}{2} \\ \int_0^{\theta_\theta}\int_{\frac{3\tau_r - \beta_{pmz} - \alpha_{sz}}{2} - z_1}^{\delta} \dfrac{\mu_0 dr_z d\theta}{\pi r_z + g} \quad \tau_r - \dfrac{\alpha_{sz}}{2} < z_1 < \dfrac{3\tau_r - \beta_{pmz} - \alpha_{sz}}{2} \end{cases} \tag{11}$$

According to (10), (11), Tables I and II, the flux leakage of PM-stator pole-PM can be derived at any positions. For example, when $0<\theta_1<\pi\alpha_{sp}/2p-\pi(1-\alpha_p)/2p$ and $0<z_1<\alpha_{sz}/2-(\tau_r-\beta_{pmz})/2$, the expressions of the flux leakage magnetic permeance of PM-stator pole-PM in the circumferential and axial directions are

$$P_{psp\theta}(\theta_1, z_1) = \int_0^{\frac{\alpha_{sz}-(\tau_z-\beta_{pmz})}{2}} \int_0^{\frac{\delta}{R_m}} \frac{\mu_0 R_m d\theta dz}{\pi R_m \theta + g} \tag{12}$$

$$= \mu_0(\alpha_{sz} - \tau_z + \beta_{pmz})/2\pi \ln[(\pi\delta + g)/g]$$

$$P_{pspz}(\theta_1, z_1) = \int_0^{\frac{\pi(\alpha_{sp}-1+\alpha_p)}{2p}} \int_0^{\delta} \frac{\mu_0 dr_z d\theta}{\pi r_z + g} = \frac{\mu_0(\alpha_{sp}-1+\alpha_p)}{2p} \ln\frac{\pi\delta + g}{g} \tag{13}$$

TABLE I
CORRESPONDING RELATIONSHIP OF z_1 AND z_z

Range of z_1	z_z
$(0, \alpha_{sz}/2-(\tau_r-\beta_{pmz})/2)$	$\alpha_{sz}/2-(\tau_r-\beta_{pmz})/2$
$(\alpha_{sz}/2-(\tau_r-\beta_{pmz})/2, \alpha_{sz}/2)$,	$\alpha_{sz}/2-(\tau_r-\beta_{pmz})/2+z_1$
$(\alpha_{sz}/2, \alpha_{sz}/2+(\tau_r-\beta_{pmz})/2)$	$3\alpha_{sz}/2-(\tau_r-\beta_{pmz})/2-z_1$
$(\alpha_{sz}/2+(\tau_r-\beta_{pmz})/2, \beta_{pmz}+(\tau_r-\beta_{pmz})/2-\alpha_{sz}/2,)$	α_{sz}
$(\beta_{pmz}+(\tau_r-\beta_{pmz})/2-\alpha_{sz}/2, \tau_r-\alpha_{sz}/2)$	$\alpha_{sz}/2-(\tau_r-\beta_{pmz})/2+\tau_r-z_1$
$(\tau_r-\alpha_{sz}/2, \tau_r+(\tau_r-\beta_{pmz})/2-\alpha_{sz}/2)$	$\alpha_{sz}/2+(\tau_r-3\beta_{pmz})/2-z_1$
$(\tau_r+(\tau_r-\beta_{pmz})/2-\alpha_{sz}/2, \tau_r)$	$\alpha_{sz}/2-(\tau_r-\beta_{pmz})/2$

TABLE II
CORRESPONDING RELATIONSHIP OF θ_1 AND θ_z

Range of θ_1	θ_z
$(0, \pi\alpha_{sp}/2p-\pi(1-\alpha_p)/2p)$	$\pi\alpha_{sp}/2p-\pi(1-\alpha_p)/2p$
$(\pi\alpha_{sp}/2p-\pi(1-\alpha_p)/2p, \pi\alpha_{sp}/2p)$	$\pi\alpha_{sp}/2p-\pi(1-\alpha_p)/2p+z_1$
$(\pi\alpha_{sp}/2p, \pi\alpha_{sp}/2p+\pi(1-\alpha_p)/2p)$	$3\pi\alpha_{sp}/2p-\pi(1-\alpha_p)/2p-z_1$
$(\pi\alpha_{sp}/2p+\pi(1-\alpha_p)/2p, \pi\alpha_p/p+\pi(1-\alpha_p)/2p-\pi\alpha_{sp}/2p)$	$\pi\alpha_{sp}/p$
$(\pi\alpha_p/p+\pi(1-\alpha_p)/2p-\pi\alpha_{sp}/2p, \pi/p-\pi\alpha_{sp}/2p)$	$\pi\alpha_{sp}/2p-\pi(1-\alpha_p)/2p+\tau_r-z_1$
$(\pi/p-\pi\alpha_{sp}/2p, \pi/p+\pi(1-\alpha_p)/2p-\pi\alpha_{sp}/2p)$	$\pi\alpha_{sp}/2p+\pi(1-3\pi\alpha_p)/2p-z_1$
$(\pi/p+\pi(1-\alpha_p)/2p-\pi\alpha_{sp}/2p, \pi/p)$	$\pi\alpha_{sp}/2p-\pi(1-\alpha_p)/2p$

Then the reluctance ($R_{pM\theta}$, R_{pMz}, $R_{pp\theta}$, R_{ppz}, $R_{psp\theta}$, R_{pspz}) can be obtained by taking the reciprocal of the magnetic permeance in (6)-(11). Fig. 6 shows the magnetic circuit of single stator pole model for flux leakage calculation, which is shown in Fig. 5 (a). R_{m01}, R_{m02}, R_{m03} and R_{m04} are the reluctances of PM pole corresponding to stator pole, respectively. $R_{pM\theta1}$, R_{pMz1}, $R_{pM\theta2}$, R_{pMz2}, $R_{pM\theta3}$, R_{pMz3}, $R_{pM\theta4}$ and R_{pMz4} are the leakage reluctances of PM pole to the mover corresponding to stator pole in circumferential and axial directions, respectively. $R_{pp\theta1}$, R_{ppz1}, $R_{pp\theta2}$ and R_{ppz2} are the leakage reluctances of between the adjacent PM poles in circumferential and axial directions, respectively. $R_{psp\theta1}$, R_{pspz1}, $R_{psp\theta2}$ and R_{pspz2} are the leakage reluctances of between the adjacent PM poles and stator pole in circumferential and axial directions, respectively.

According to the magnetic circuit model, the expressions of the air gap main flux and total flux of each pole are

$$\frac{\phi_r - \phi_\delta}{R_\delta \phi_\delta} = \frac{1}{R_{m0}} + \frac{1}{R_{pM\theta}} + \frac{1}{R_{pMz}} + \frac{1}{R_{pp\theta}} + \frac{1}{R_{psp\theta}} + \frac{1}{R_{ppz}} + \frac{1}{R_{pspz}} \tag{14}$$

$$\frac{\phi_m - \phi_\delta}{R_\delta \phi_\delta} = \frac{1}{R_{pM\theta}} + \frac{1}{R_{pMz}} + \frac{1}{R_{pp\theta}} + \frac{1}{R_{psp\theta}} + \frac{1}{R_{ppz}} + \frac{1}{R_{pspz}} \tag{15}$$

$$(\phi_r - \phi_m)R_{m0} = R_\delta \phi_\delta \tag{16}$$

where ϕ_r is the intrinsic flux of PM, ϕ_m is the total flux provided by PM to external magnetic circuit, ϕ_δ is the air gap main flux in a pole pitch, and R_δ is the air gap reluctance per pole, the actual values of ϕ_r, ϕ_m, ϕ_δ, R_δ, R_{m0}, $R_{pM\theta}$, R_{pMz}, $R_{pp\theta}$, R_{ppz}, $R_{psp\theta}$ and R_{pspz} are related with the relative position of the stator and the mover.

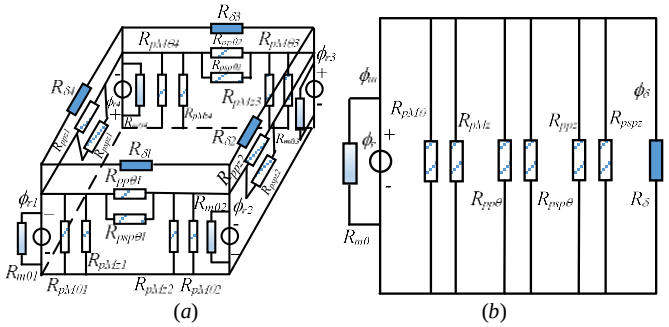

Fig. 6. Magnetic circuit of single stator pole for flux leakage calculation, (a) magnetic circuit, and (b) simplified magnetic circuit.

The expressions of PM reluctance and air gap reluctance are

$$R_{m0} = h_m / \mu_0 \mu_r S_m \tag{17}$$

$$R_\delta = \delta / \mu_0 S_{eff} \tag{18}$$

where μ_r is the PM relative permeability, μ_0 is the vacuum permeability, S_m is the cross-sectional area in magnetizing direction of PM, $S_m = \beta_{pmz} R_m \alpha_p \pi / p$, S_{eff} is the air gap effective cross-sectional area for consideration of edge effect, and $S_{eff} = (\beta_{pmz} + \delta)(R_m \alpha_p \pi / p + \delta)$. h_m is the length of PM in magnetization direction. $\delta = k_\delta g$, where k_δ is the Carter factor.

In order to acquire the relationship between the tooth flux and the rotor position, the stator tooth pitch is divided into n segments. After the mover has rotated by a stator tooth pitch, namely, the flux of every tooth is calculated at n different positions. Fig. 7 shows the maximum value of the main flux and side flux waveforms of stator pole of phase A compared with the total flux of E-shape stator when it works in rotary motion or linear motion. It is seen that the maximum values of the main flux and side flux are 1.24×10^{-4} Wb and 2.17×10^{-5} Wb, respectively. The total side flux waveform of the E-shape stator is sinusoidal whether it works in rotary or linear motion. However, the main flux waveforms are sinusoidal and trapezoid waves when the motor works in rotary and linear motions, respectively. The angular velocities of main flux and total side flux are equal to those of the mover while it works in

rotary motion, while the angular velocity of total side flux is equal to three times of that of the mover when it works in linear motion, which is consistent with the results of (4).

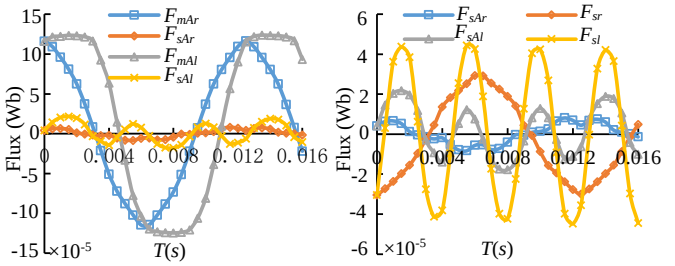

Fig. 7. Main and side flux waveforms, (a) main flux and side flux of phase A, and (b) side flux of phase *A* compared with the total side flux of E-shape stator when it works in rotary or linear motion.

IV. Optimization Design

A. Calculation of back EMF

Taking E-shape stator as the smallest unit of analysis, the stator tooth flux can be calculated at different times when the mover is in different positions. The flux linkage can be obtained according to the relationship between the PM poles and stator tooth. Then the back EMF is generated by the flux change of the windings. The expression of back EMF is

$$u = \omega_\theta \frac{d\psi}{d\theta} + \omega_z \frac{d\psi}{dz} = 2\pi f_\theta \frac{d\psi}{d\theta} + 2\tau f_z \frac{d\psi}{dz} \tag{19}$$

where ω_θ and ω_z are the angular frequencies of circumferential and axial back EMFs, respectively. f_θ and f_z are the frequencies of circumferential and axial back EMFs, respectively.

After the flux is obtained at different mover positions, the first element of the back EMF vector and the back EMF at the first position can be calculated by

$$e_{(m,n)} = 2\pi f_r \frac{\psi_{m+1} - \psi_m}{\theta_{m+1} - \theta_m} + 2\tau f_z \frac{\psi_{n+1} - \psi_n}{z_{n+1} - z_n} \tag{20}$$

B. Calculation of Cogging Torque and Detent Force

Assuming that the permeability of iron is infinite, there is only the normal component of the magnetic flux density at the interface between the stator teeth and the air gap. When the magnetic flux lines enter the stator core, they are perpendicular to the tooth surface.

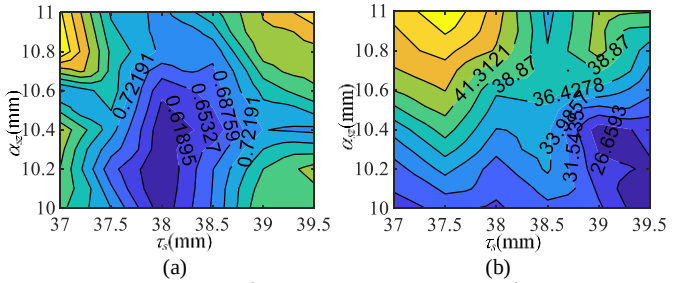

Fig. 8. The contour map of cogging torque and detent force, (a) cogging torque (Nm), and (b) detent force (N).

According to (2), the analysis results of the relative magnetic permeance in [4] and Maxwell stress tensor method, Fig. 8 shows the cogging torque and detent force of IPM-LRM with different α_{sz} and τ_s. α_{sz} and τ_s are the stator pole width and stator pole pitch in axial direction, respectively. The values of α_{sz} and τ_s can be decided by considering the cogging torque and detent force. When the range of α_{sz} is (10mm, 11mm) and the range of τ_s is (37.5mm, 39.5mm), the cogging torque and detent force can both meet the design requirement. Based on the previous analysis, the main parameters of the motor are decided, which are listed in Table III.

TABLE III
MAIN PARAMETERS OF THE TOPOLOGY

Parameters	Value	Parameters	Value	Parameters	Value
R_r	19.2mm	L_a	88.4mm	R_m	22.2mm
R_s	22.8mm	β_{pmz}	25.1mm	$\beta_{pm\theta}$	11.6mm
$\alpha_{s\theta}$	11.2mm	τ	29.1mm	τ_s	38.8mm
α_{sz}	10.8mm	w_{sp}	17.2mm	w_{sy}	11mm
h_m	3mm	g	0.6mm	N	150

According to (20), Fig. 9 shows the back EMF waveforms of phase *D* when the motor is in rotary and linear motions, which are analyzed by analytical method and 3D FEM. It is noticed that the results analyzed by analytical method are consistent with the results analyzed by 3D FEM.

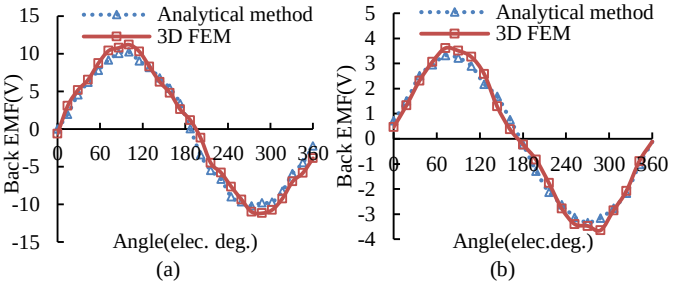

Fig. 9. Back EMF waveforms when the motor works in (a) rotary motion, and (b) linear motion.

V. Conclusion

In order to reduce the difficulty of the optimization of IPM-LRM, the flux in the E-shape stator section of LRPMM is analyzed in the paper. The main flux is calculated by analytical method. The variation law of the total side flux of E-shape stator is derived and concluded, namely, the angular velocities of main flux and total side flux of E-shape stator are equal to those of the mover while the motor works in rotary motion, while the angular velocity of the total side flux of E-shape stator is equal to three times of that of the mover when it works in linear motion. Since the flux leakage of the motor varies periodically, only one of the stator teeth of the E-shape stator will have the maximum flux leakage when the motor is in rotary or linear motion. In this paper, the flux leakage is divided into PM-PM leakage, PM-mover leakage and PM-stator pole-PM leakage, which is analyzed by MCM. According to the calculation of the flux leakage and the side flux, the flux of the single stator pole can be derived and the back EMF is optimized. The cogging torque and detent force are taken as the constraint conditions of the optimal design, then the optimum value of the motor structure is obtained.

ACKNOWLEDGMENT

This work was supported by the Natural Science Foundation of China under Grant 51905003, Natural Science Foundation of Anhui Province under Grant 1908085QE207, and China Postdoctoral Science Foundation under Grant 2019M652161.

REFERENCES

[1] Z. Song, C. Liu, K. Feng, H. Zhao, and J. Yu, "Field prediction and validation of a slotless segmented-Halbach permanent magnet synchronous machine for more electric aircraft," *IEEE Trans. Trans. Electrif.*, vol. 6, no. 4, pp. 1577-1591, Dec. 2020.

[2] A. Mollaeian, E. Ghosh, H. Dhulipati, J. Tjong, and N. C. Kar, "3-D sub-domain analytical model to calculate magnetic flux density in induction machines with semiclosed slots under no-load condition," *IEEE Trans. Magn.*, vol. 53, no. 6, pp. 1-5, June 2017.

[3] P. Jin, H. Lin, S. Fang, Y. Yuan, Y. Guo, and Z. Jia, "3-D analytical linear force and rotary torque analysis of linear and rotary permanent magnet actuator," *IEEE Trans. Magn.*, vol. 49, no. 7, pp. 3989-3992, July 2013.

[4] P. Jin, S. Fang, H. Lin, Z. Q. Zhu, Y. Huang, and X. Wang, "Analytical magnetic field analysis and prediction of cogging force and torque of a linear and rotary permanent magnet actuator," *IEEE Trans. Magn.*, vol. 47, no. 10, pp. 3004-3007, Oct. 2011.

[5] K. Guo and Y. Guo, "Design optimization of linear-rotary motion permanent magnet generator with E-shaped stator," *IEEE Trans. Appl. Supercond.*, vol. 31, no. 8, Nov. 2021, Art no. 0600705.

[6] L. Wu, H. Yin, D. Wang, and Y. Fang, "A nonlinear subdomain and magnetic circuit hybrid model for open-circuit field prediction in surface-mounted PM machines," *IEEE Trans. Energy Convers.*, vol. 34, no. 3, pp. 1485-1495, Sept. 2019.

[7] S. Li, S. Zhang, J. Dang, T. G. Habetler, and R. G. Harley, "Analytical calculation of the phase inductance profile of switched reluctance machines," *IEEE Trans. Energy Convers.*, vol. 34, no. 3, pp. 1149-1163, Sept. 2019.

[8] H. Chen, C. Sun, and Q. Wang, "Analysis of flux-linkage characteristics of switched reluctance linear generator," *IEEE Trans. Appl. Supercond.*, vol. 24, no. 3, Jun. 2014, Art. 5000105.

[9] O. Misir, S. M. Raziee, and B. Ponick, "Determination of the inductances of salient pole synchronous machines based on the voltage equation of a single coil in the stator winding," *IEEE Trans. Ind. Appl.*, vol. 52, no. 5, pp. 3792-3804, Oct. 2016.

[10] R. Qu and T. A. Lipo, "Analysis and modeling of air-gap and zigzag leakage fluxes in a surface-mounted permanent-magnet machine," *IEEE Trans. Ind. Appl.*, vol. 40, no. 1, pp. 121-127, Feb. 2004.

[11] W. Li, K. T. Chau, C. Liu, S. Gao, and D. Wu, "Analysis of tooth-tip flux leakage in surface-mounted permanent magnet linear vernier machines," *IEEE Trans. Magn.*, vol. 49, no. 7, pp. 3949-3952, Jul. 2013.

[12] P. Gao, Y. Gu, S. H. Shah, U. Abubakar, and X. Wang, "Calculation and analysis of flux leakage coefficient of interior permanent magnet synchronous motors with fractional slot concentrated windings," *IEEE Trans. Appl. Supercond.*, vol. 29, no. 2, Mar. 2019, Art. 0602004.